The Role of Body Wall Muscles in *C. elegans* Locomotion

Jordan Boyle and Netta Cohen
School of Computing, University of Leeds, Leeds LS2 9JT, UK

Abstract

Over the past four decades, one of the simplest nervous systems across the animal kingdom, that of the nematode worm *C. elegans*, has drawn increasing attention. This system is the subject of an intensive concerted effort to understand the behaviour of an entire living animal, from the bottom up and the top down. *C. elegans* locomotion, in particular, has been the subject of a number of models, but there is as yet no general agreement about the key (rhythm generating) elements. In this paper we investigate the role of one component of the locomotion subsystem, namely the body wall muscles, with a focus on the role of inter-muscular gap junctions. We construct a detailed electrophysiological model which suggests that these muscles function, to a first approximation, as mere actuators and have no obvious rhythm generating role. Furthermore, we show that within our model inter-muscular coupling is too weak to have a significant electrical effect. These results rule out muscles as key generators of locomotion, pointing instead to neural activity patterns. More specifically, the results imply that the reduced locomotion velocity observed in unc-9 mutants is likely to be due to reduced neuronal rather than inter-muscular coupling.

Key words: *Caenorhabditis elegans* locomotion, body wall muscles, gap junctions, conductance based models

1. Introduction

Over more than a century, huge advances have been made in understanding the operation of neurons at a cellular and sub-cellular level, as well as in abstractly understanding the operation of large scale neural networks, such as those found in mammalian cortex. However, despite these impressive advances, we have yet to succeed in fully understanding the neural basis of all but the simplest behaviours. One organism, *Caenorhabditis elegans*, provides us with the first tangible possibility of understanding complex behaviours of an organism from the genetic and molecular level, through the cellular level, right up to the system level (and back down).

C. elegans is a small (about 1mm long) nematode worm [1], which has been the subject of much scientific research over the years. It is extensively used as a model organism for genetic research, due in part to its short life cycle and fully sequenced genome [2]. In addition, it is an attractive subject for research on the neural basis of behaviour due to an invariant nervous system consisting of a mere 302 neurons in the adult hermaphrodite. While the connectivity of its nervous system is known to an unprecedented degree of accuracy, far less information is available on the electrical properties of these neurons. Thus the question of the neural basis of *C. elegans* behaviour is still an open and attractive one.

1.1. *C. elegans locomotion*

C. elegans movement typically consists of periods of forward motion interspersed with short periods of backward motion and turns. Forwards and backwards locomotion are achieved by propagating sinusoidal undulations along the body from head to tail (or tail to head) respectively. The worm's locomo-

Email address: netta@comp.leeds.ac.uk (Netta Cohen).

tion is controlled by a small, known subset of its nervous system [3], and manipulations at the genetic or neuronal level allow insight into its inner workings. The apparent modularity of this subsystem, along with its easily observable output, make the locomotion nervous system a particularly appealing subject for modelling work.

Various models of *C. elegans* locomotion have already been developed [4–9]. Nonetheless the system is still only partially understood, and remains of significant interest to modellers and experimentalists.

One fundamental unresolved question is whether the rhythmic motor control of forward locomotion relies on a central pattern generator (CPG) circuit or on sensory feedback. The conventional wisdom (supported by all evidence to date) is that all rhythmic motor behaviours across the animal kingdom are produced by CPGs, but such a CPG has been elusive in the *C. elegans* locomotion circuit [7,8]. Thus, some models [4,7] propose a mechanism whereby undulations are activated by stretch receptors that provide sensory feedback from body posture, with no intrinsic neuronal oscillator. One possible issue with regard to any locomotion model in the worm is the relatively sparse modelling work on the body wall muscles.

In particular, it is not known which components of the locomotion subsystem are actively involved in generating and shaping locomotion. The candidates are the interneurons, ventral cord motorneurons, body wall muscles and the *C. elegans* body itself. Putting aside the possible contribution of the body (but see [4,5,7,8]), the two alternatives are either that the patterned activity of the motor neurons activate the muscles which then act as actuators to deliver the mechanical contractions, or, perhaps more interestingly, that in addition to neuronal activity, the muscles themselves are capable of generating oscillatory dynamics and/or of propagating such signals down the length of the worm. The former holds in most studied motor systems: the neural ciruit generates a patterned output, and the muscles serve as actuators of that output. Interestingly, this does not appear to be the case in *Ascaris lumbricoides* [10,4] – a much larger but closely related nematode whose nervous system is structurally very similar to that of *C. elegans*.

In *Ascaris*, the body wall muscles are electrically coupled by gap junctions [1] and appear to form a functional syncytium which produces spontaneous myogenic activity: graded spikes superimposed on slow depolarisations, which propagate independently of the nervous system [10]. From this perspective, it may not be surprising if *C. elegans* muscles had a similar pattern generating (or pattern modulating) role in locomotion.

In the absence of a direct answer to this question, one may turn to behavioural evidence from locomotion-defective (or so called uncoordinated) mutant strains of the worm. Particularly instructive are mutations that might disrupt electrical signal flow between muscles. There are two known gap junction genes in *C. elegans* namely unc-7 and unc-9, mutations of which result in virtually identical phenotypes [11] where locomotion is severely impaired. Both are widely expressed, but only unc-9 is expressed in muscles. In Ref. [12] it is shown that worms treated with unc-9 RNA interference (RNAi) to suppress unc-9 gene expression exhibit substantially reduced locomotion velocities, and the authors suggest that this effect should be attributed specifically to the reduction in gap junction coupling between body wall muscles.

In this paper, we rely on electrophysiological data recorded from body wall muscles *in vitro* to construct a model of individual and coupled muscle cells. We then use this model to determine what possible active role may be attributed to individual *C. elegans* body wall muscles and, furthermore, to determine the consistency of such a model with the observed unc-9 phenotype. More specifically, we attempt to address the following questions: Do the muscles exhibit action potentials? What is their contribution to the generation of rhythmic behaviour? And finally, how strong is the inter-muscular coupling, and to what extent does it affect locomotion?

1.2. *Typical effects of diffusive coupling*

Gap junctions are found in a range of organs and cell types in vertebrates as well as invertebrate species and are very common in excitable tissue (e.g., heart muscle, pancreas, and the brain). Many gap junctions have fixed conductances and act as resistive elements. The current flowing through such a resistor would be proportional to the voltage drop across it, or the potential difference between the two coupled cells, j and k: $I_{j,k} = G\,(V_k - V_j)$

[1] Gap junctions, or electrical synapses, are non-selective channels that form between two adjacent cells, allowing ions and small molecules to pass between the them.

where G denotes a constant conductance (or inverse resistance). In *C. elegans*, it appears that the conductance of some gap junctions is itself a function of the potential difference between the coupled cells. Nonetheless, for the purposes of this introduction, suffice it to consider whether the coupling is relatively 'weak' or 'strong', neglecting any functional dependence of the conductance.

If coupling is sufficiently strong, the coupled elements will fully synchronise. Therefore the more interesting cases are those of weak and intermediate coupling. Weakly coupled limit cycle oscillators have been the subject of much theoretical investigation [13–15]. Typically, the frequencies of the oscillators are pulled towards each other, and full or partial entrainment may result, depending on the difference in natural frequency and the strength of the coupling. In certain situations unexpected behaviour can result, such as antiphase oscillation [16], bursting [17] and even quenching [18].

Coupling between non-oscillating elements has received less attention, but here one would expect two main effects. First, gap junctions will allow diffusive currents to diminish potential differences between coupled cells. In addition, the input impedance of the cells will be affected altering their frequency response [19].

2. Methods

The body wall muscles of *C. elegans* are divided into four quadrants, two ventral and two dorsal, each quadrant consisting of 23 or 24 trapezoidal cells, arranged in two staggered rows. When it locomotes, the worm lies on its side, with the pairs of ventral and dorsal muscle quadrants contracting in unison. Gap junctions couple cells within each quadrant, as well as between quadrants, on either the ventral or dorsal sides. Within a quadrant, gap junctions are found between each muscle cell and the two overlapping cells from the other row [12]. In the work that follows, we have reduced each muscle quadrant to a chain of identical cells with nearest neighbour coupling.

Nematode muscles are unusual in that they extend thin, non-contractile processes to the nerve cord, where they receive their neuromuscular input. Gap junctions are found between these muscle arms, coupling cells from the two ventral (or dorsal) quadrants. Each muscle typically has three to five arms [20]. We developed a compartmental conductance based model, with one compartment for the cell body and ten compartments for each muscle arm. All active currents are included in the main compartment, while the arms are modelled as passive cables.

2.1. *Electrical properties of the muscle body*

We began by developing a conductance based model of the muscle body. The model contains three active currents [21,22]: fast and slow potassium currents (I_{Kf} and I_{Ks}) and a calcium current (I_{Ca}) that exhibits inactivation on both fast and slow timescales, mediated by Ca^{2+} and voltage respectively. We also include a standard leak conductance I_L. A circuit diagram of the complete model is shown in Figure 1. The membrane potential for the i_{th} muscle in the chain is therefore given by

$$\begin{aligned} C\frac{dV_i}{dt} &= -\Sigma I_{\text{ion}} + I_{\text{in}} + I_{i-1,i} + I_{i+1,i} \\ \Sigma I_{\text{ion}} &= I_{Ks} + I_{Kf} + I_{Ca} + I_L \,, \end{aligned}$$

where I_{in} is the input current from the muscle arms (see Section 2.2) and $I_{j,k}$ are gap junction currents (see Section 1.2). The membrane currents are given by

$$\begin{aligned} I_{Ks} &= g_{Ks} n (V - V_{Ks}) \\ I_{Kf} &= g_{Kf} p^4 q (V - V_{Kf}) \\ I_{Ca} &= g_{Ca} e^2 f (1 + (h-1)\alpha_{Ca})(V - V_{Ca}) \\ I_L &= g_L (V - V_L) \,, \end{aligned}$$

with activation variables e, n, p, and inactivation variables f, h, q. Gating kinetics are given in terms of a generic variable x

$$\frac{dx}{dt} = \frac{x_\infty(V, V_{\text{half}(x)}, k_{(x)}) - x}{\tau_x}$$

with a steady state given by

$$x_\infty(X, X_{\text{half}}, k) = \frac{1}{1 + \exp\left[\frac{X_{\text{half}} - X}{k}\right]} \,,$$

and the calcium mediated inactivation is given by

$$h = x_\infty([Ca^{2+}]_i, Ca_{\text{half}(h)}, k_{(h)}).$$

In order to find values for the 29 parameters of this model we simulated voltage clamp and current clamp traces of the model, fitting the parameters to corresponding whole cell recordings of body wall muscle cells *in vitro* [22]. We similarly fit the steady state I-V curves for I_K and I_{Ca} [21,22]. Parameters for which values were reported in the literature were

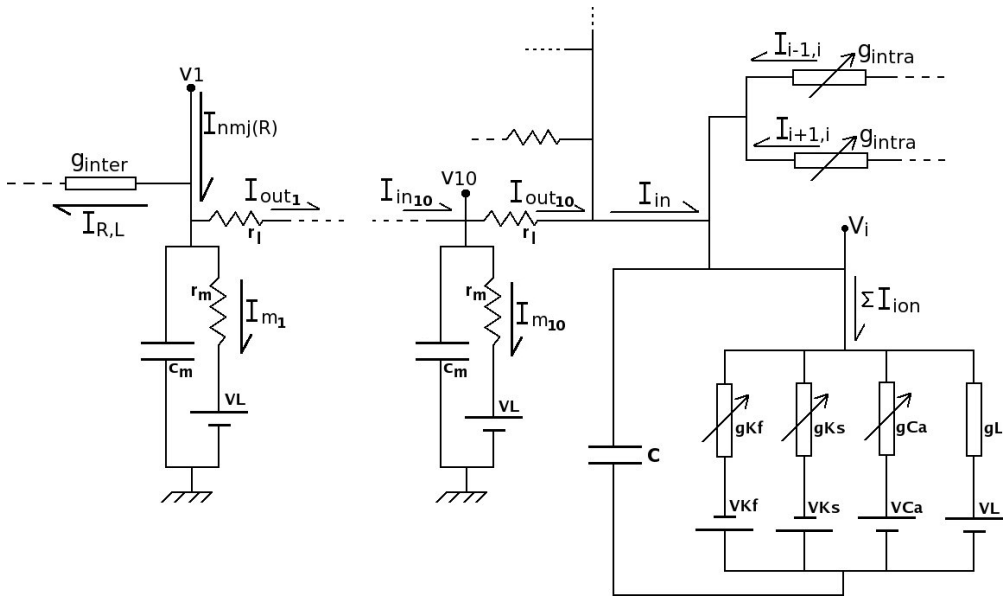

Fig. 1. Equivalent circuit diagram of the muscle model showing currents, voltages and parameters of the muscle body (bottom right of figure), muscle arms (with two of ten compartments of one arm shown and remaining arms appearing in parallel) and coupling. All labels correspond to those in the text.

limited to a range close to the reported values. Fits were obtained by an evolutionary algorithm (differential evolution [23]). The parameters obtained are given in Appendix A. Note that the value of $C = 30pF$ was not evolved, but was taken from [12] and used for compatibility with coupling parameters. All simulations were run with a 4_{th} order Runge-Kutta method with a time step of $0.1ms$.

2.2. *Muscle arms*

The muscles arms are modelled as passive cables, each characterised by membrane capacitance (c_m), membrane resistance (r_m) and longitudinal resistance (r_l) (see Figure 1). We used $N = 10$ discrete compartments for each arm, with 5 arms per muscle. The membrane potential of each arm compartment evolves according to

$$c_m \frac{dv_n}{dt} = I_{\text{in}_n} - I_{\text{out}_n} - I_{m_n} \quad \text{for} \quad n = 1 : N,$$

where I_{in_n} is the current flowing into the n_{th} compartment, I_{out_n} is the current flowing out of the n_{th} compartment and I_{m_n} is the current leaking through the cell membrane, according to

$$I_{m_n} = \frac{v_n - V_L}{r_m} \quad \text{for} \quad n = 1 : N.$$

The current flowing out of compartment n into compartment $n + 1$ is

$$I_{\text{out}_n} = \frac{v_n - v_{n+1}}{r_l} \quad \text{for} \quad n = 1 : N - 1$$
$$I_{\text{out}_N} = \frac{v_N - V}{r_l},$$

where V is the membrane potential of the muscle body. With the exception of the first compartment, the current that flows out of one compartment must flow into the next, so

$$I_{\text{in}_n} = -I_{\text{out}_{n-1}} \quad \text{for} \quad n = 2 : N.$$

For two coupled muscles (whether on the dorsal or ventral side), the first compartment of arms on the right (left) muscle quadrant

$$I_{\text{in}_1} = I_{\text{nmj}} \pm I_{R,L},$$

where I_{nmj} is the neural input, and $I_{R,L}$ is the inter-quadrant gap junction current described in Section 2.3. Finally, the total current flowing into the muscle body is the sum of currents flowing out of each of the five arms

$$I_{\text{in}} = -\Sigma I_{\text{out}_N}.$$

Since no data on the electrical properties of the arms could be found, the cable parameters were based on estimates of the specific capacitance (C_m) and resistance (R_m) of the membrane, and the specific resistance of the cytoplasm (R_l), scaled by the arm dimensions. This is described in more detail, along with a table of the parameters, in Appendix A.

2.3. *Coupling*

The inter-muscular gap junctions are described in [12]. The intra-quadrant gap junction conductance is a function of the potential difference across the junction, while coupling between quadrants has no voltage dependence (and a significantly smaller conductance). The intra-quadrant gap junction current introduced in Section 2.1 is given by

$$I_{j,k} = G_{ss}(V_j - V_k)(V_j - V_k),$$

where

$$G_{ss}(\Delta V) = g_{\text{intra}} \left[\frac{1 - G_{\min}}{1 + \exp(A(|\Delta V| - V_0))} + G_{\min} \right].$$

The inter-quadrant coupling from Section 2.2 is simply

$$I_{R,L} = g_{\text{inter}}(v_1(R) - v_1(L)),$$

where $v_1(R)$ is the potential of the first compartment of a right muscle arm and $v_1(L)$ is the potential of the first compartment of a left muscle arm.

2.4. *Current stimuli*

Inter-quadrant coupling occurs between cells that should be coactive (either on the ventral or dorsal side). To investigate whether these gap junctions could contribute to equalising input to left and right muscles, we stimulate the arms of the right muscle with a constant current step and monitor the resulting potential change in both left and right muscle bodies.

Intra-quadrant coupling is different, as it occurs between cells which would be expected to have slightly different input. The locomotion waveform is periodic in time, with a frequency of about $0.5Hz$. It is also periodic in space, with a wavelength of approximately $\frac{2}{3}$ of body length on agar. Therefore the inputs to adjacent muscles should be phase shifted by approximately $\frac{2\pi}{\frac{2}{3}24} = \frac{\pi}{8}$. It has been shown that the related nematode *Ascaris* has non-spiking neurons and graded synaptic transmission [24]. We will make the common assumption that *C. elegans* motorneurons share these properties. We therefore expect the current input to each muscle to be some smoothly varying function. The results from two such functions are shown in Section 3.3. Similar results were obtained for all other waveforms tested.

2.5. *Signal-to-noise ratio*

Another potential effect of coupling is on signal-to-noise ratio (SNR). Synaptic vesicle release is a stochastic process, so real neuromuscular currents are likely to have a random component. Rather than explicitly modelling vesicle release, we have used an approximation where input to each muscle consists of a periodic signal combined with additive white Gaussian (zero-mean) noise. The method used for estimating the SNR of a signal is described in Appendix B.

3. Results

3.1. *Behaviour of the single cell model*

Figure 2 shows the experimental voltage- and current-clamp traces [22] along with corresponding traces produced by simulation of our model with matching inputs. Likewise Figure 3 shows I-V curves for I_K and I_{Ca} (recorded and simulated). The model output is quantitatively very similar to the experimental data.

In contrast to *Ascaris* body wall muscles [25], our model muscles do not produce spikes, either spontaneously or in response to current injection. Even when the fitness function for the parameter optimisation was altered to specifically reward oscillatory behaviour, spiking could not be achieved for realistic values of g_{Ca}. While the non-spiking nature of the muscles may be surprising, it is consistent with behaviour of the muscles *in vitro* [26]. The steady state I-V curve for an entire model muscle cell is shown in Figure 4. The voltage response diminishes as current increases, giving the muscles a wider dynamic range.

3.2. *Propagating activity*

A key question is whether the combination of active, excitatory currents and electrical coupling might allow regenerative propagation of activity down the chain of muscles, as reported in *Ascaris* [10]. Not only does the absence of spikes make this unlikely, but the coupling is also insufficiently strong. Experiments with our model suggest that an increase of four fold in g_{Ca} and about six fold in g_{intra} would be required to allow regenerative propagation (not shown).

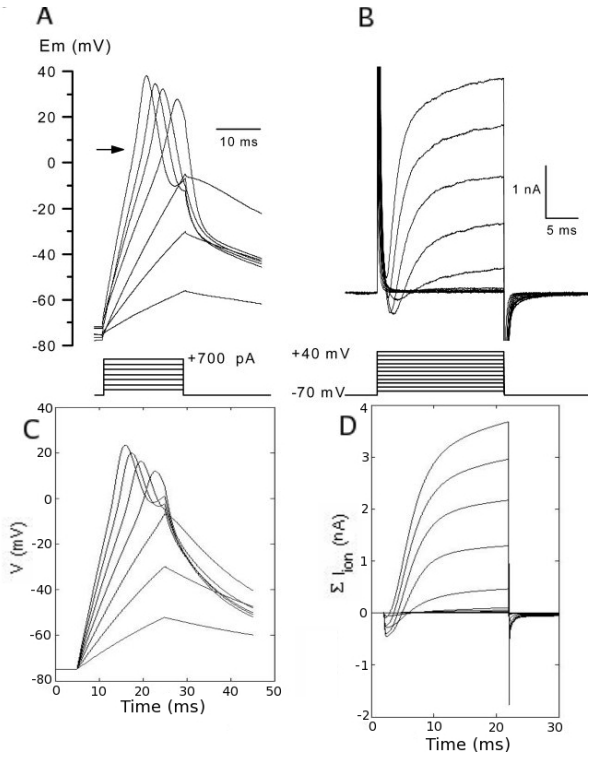

Fig. 2. Whole cell current (A) and voltage (B) clamp traces from body wall muscle cells reproduced with permission from [22], with stimulus protocols shown below the traces. The response of our model muscle cells to identical stimuli are shown in (C) and (D).

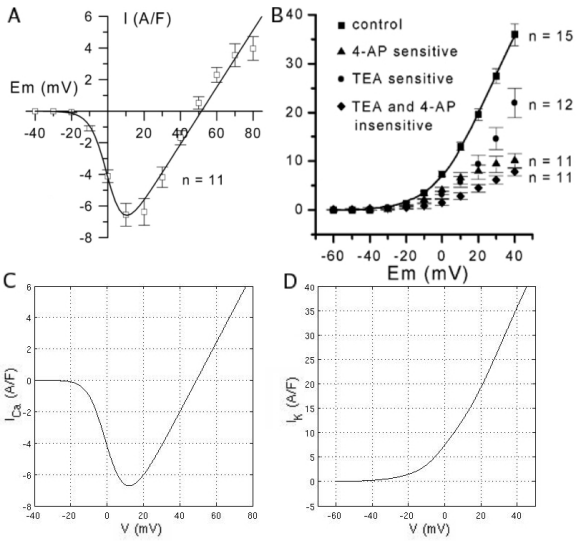

Fig. 3. Current-voltage relationships for the peak calcium (A) and steady state potassium (B) currents taken with permission from [22] and [21] respectively. Currents are shown normalised by cell capacitance. In (B), the relevant curve is the one labelled control. The corresponding relationships produced by our model are shown in (C) and (D). For technical reasons it was more convenient to compare peak calcium current and steady state potassium current.

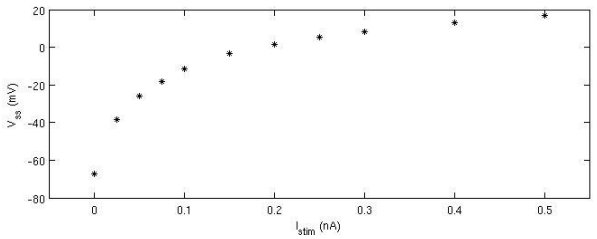

Fig. 4. Whole cell I-V curve. The cell was held at -70mV by injecting hyperpolarising current and then stimulated with $400ms$ depolarising current steps. The membrane potential at the end of the stimulus was recorded.

3.3. *Intra-quadrant coupling*

To investigate the effects of intra-quadrant coupling, we simulated a chain of 24 muscle cells with nearest neighbour coupling, as described in Sections 2.1 and 2.3. Current stimuli were applied as discussed in Section 2.4. Simulations were repeated with $g_{\text{intra}} = 0$.

Figure 5 A and B show the results of these simulations for two different input current waveforms. Traces are shown for two representative neighbouring cells from near the middle of the chain. For all the input waveforms tested, removing the coupling led to a barely noticeable change in the membrane potential traces. Looking closely, one can see that the difference in coupled and uncoupled potential becomes smaller as the cells are depolarised. Indeed, as the cells are depolarised their total membrane conductance increases, thereby making g_{intra} smaller by comparison.

As can be seen in the figure, the effect of coupling on $[Ca^{2+}]_i$ levels is generally smaller still, since changes in V below the threshold for I_{Ca} have no effect on $[Ca^{2+}]_i$. For a final test we used an input waveform specifically designed to maximise the effect on $[Ca^{2+}]_i$, applying a square wave input that (though unrealistic) maximises the potential difference across the gap junctions. We also added a depolarising bias current to give the cells a new resting potential of around $-10mV$ where the gradient in the I-V curve for I_{Ca} starts to become steep (see Figure 3). As can be seen in Figure 6, the effect of coupling on $[Ca^{2+}]_i$ is indeed much larger in this case, peaking at about 15%. However this peak is a brief transient and is followed by a negative trough of similar amplitude, so it would be unlikely to result in any behavioural change.

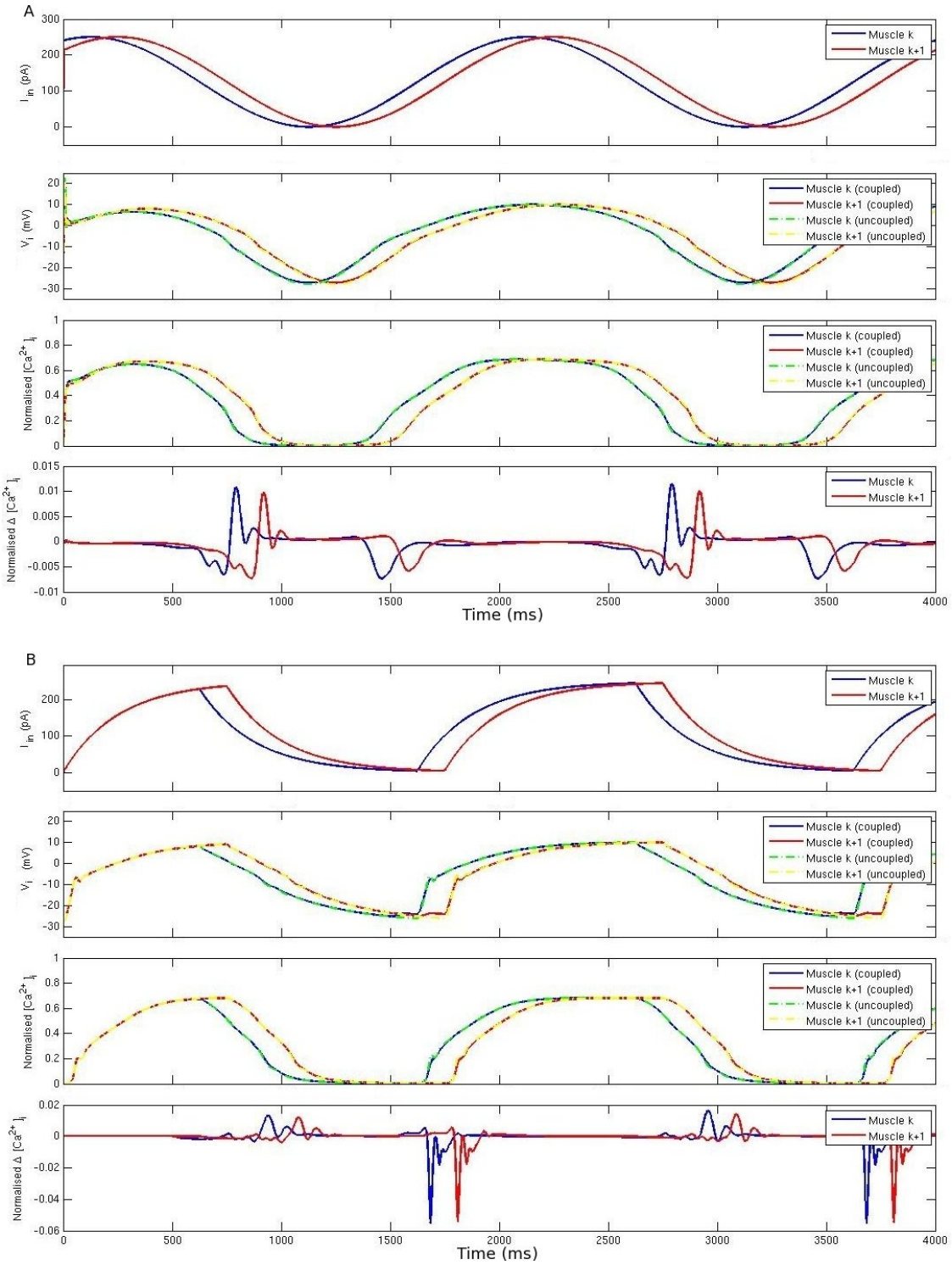

Fig. 5. The effects of intra-quadrant coupling for two possible input waveforms. Inputs are (A) sinusoidal and (B) "saw-tooth" (similar to the outputs of the neural model in Refs. [7,8]), with frequency of 0.5Hz and a phase shift of $\frac{\pi}{8}$ between adjacent cells. In each case the simulations were performed with a chain of 20 coupled cells. Each plot shows (from top) the input current, membrane potential with and without coupling, normalised internal calcium concentration ($[Ca^{2+}]_i / \max[Ca^{2+}]_i$) with and without coupling, and the difference between the coupled and uncoupled calcium concentrations ($\Delta[Ca^{2+}]_i = ([Ca^{2+}]_{i,\text{coupled}} - [Ca^{2+}]_{i,\text{uncoupled}}) / \max[Ca^{2+}]_i$) for two representative (neighbouring) cells from near the middle of the chain. Note the nearly identical waveforms with and without coupling.

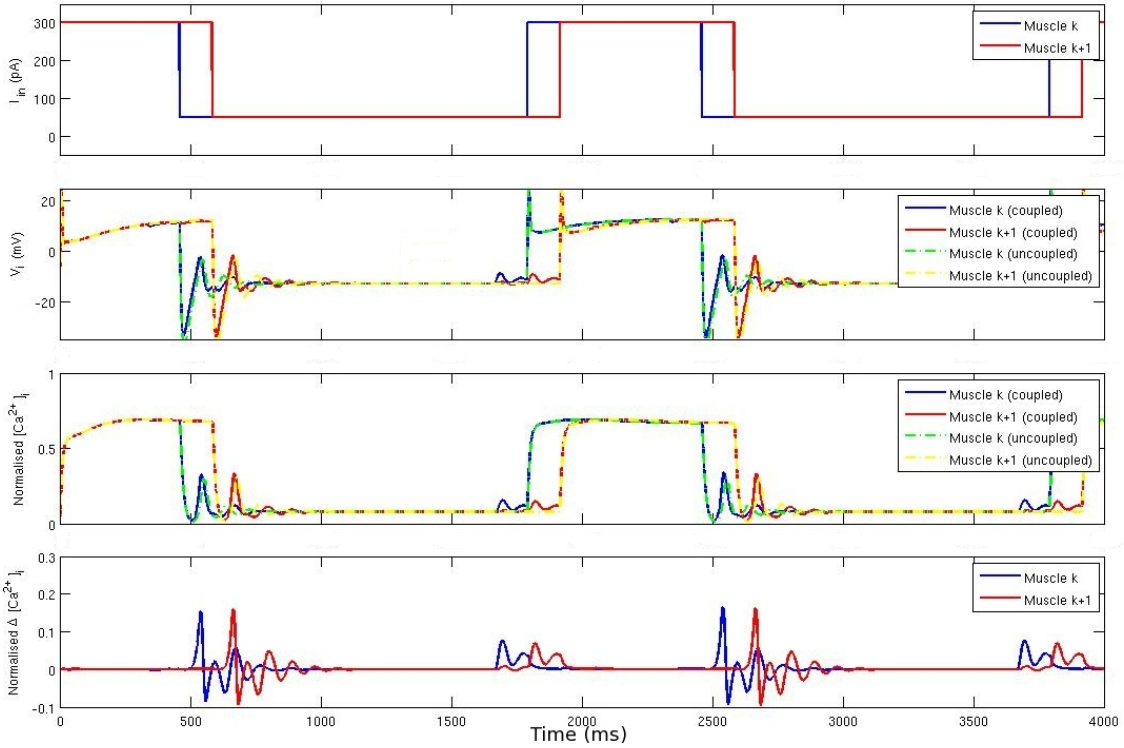

Fig. 6. Effect of intra-quadrant coupling in the most extreme case of square wave input with a depolarising bias, which increases the sensitivity of $[Ca^{2+}]_i$ to potential changes. Panels show (from top) the input current, membrane potential with and without coupling, normalised internal calcium concentration with and without coupling, and the difference between the coupled and uncoupled calcium concentrations, as in Figure 5.

3.4. *Inter-quadrant coupling*

Inter-quadrant coupling has been reported to have significantly lower conductance than intra-quadrant ($75pS$ versus $370pS$) [12]. It is plausible, however, that the location of these junctions on the tiny muscle arms might increase their significance, perhaps helping to equalise activation of muscles in the left and right quadrants. To test this possibility we simulated two cells (each with five arms as described in Section 2.2) and stimulated the arms of one muscle. The membrane potentials in the body compartments of both cells are shown in Figure 7. While the stimulated muscle responds with large depolarising steps the potential of the coupled cell is only weakly affected. When the potential of each compartment was plotted (not shown), we observed virtually no decrement in voltage down the arms, in agreement with experimental observations [27].

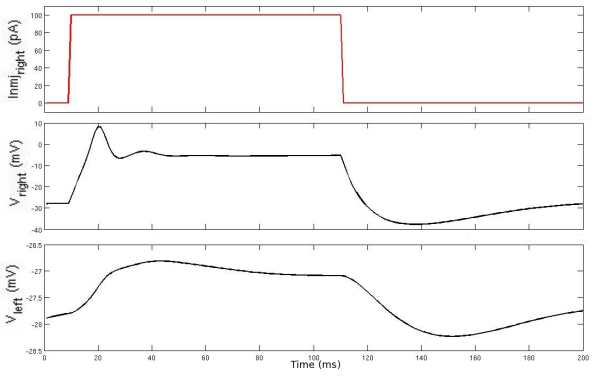

Fig. 7. Effect of inter-quadrant coupling. The right muscle arms are stimulated with a total of $100pA$ ($20pA$ per arm) for $100ms$ (top), while the left muscle arms are unstimulated. This leads to significant depolarisation of the right muscle (middle), which in turn causes current to flow through the gap junction into the left muscle arm. The resulting depolarisation of the left muscle body is just over 1mV (bottom).

3.5. *Role of coupling in noise reduction*

The cell membrane behaves much like a simple low-pass filter with time constant $\tau = \dfrac{C\text{mem}}{G\text{mem}}$. Since

G_{mem} is dynamic τ will also be. The properties of this filter will also be affected by coupling. The current stimulus used is a periodic signal with an additive noise component (as described in Section 2.5). Simulations were run both with and without coupling, for various values of noise variance σ. We then estimated the signal-to-noise ratio (SNR) of the input current and of the resulting V and $[Ca^{2+}]_i$ waveforms (as described in Appendix B).

In the absence of coupling, the low-pass characteristics of the cell leads to a significant improvement in the SNR of the membrane potential over that of the input current. The additional low-pass effect of $[Ca^{2+}]_i$ leads to an even better SNR in the calcium waveform. When coupling is added, however, there is only a very small further improvement in SNR, as illustrated in Figure 8.

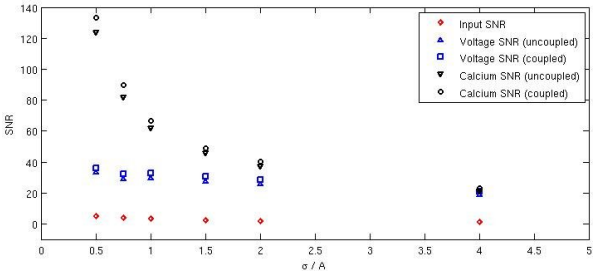

Fig. 8. Two stages of low-pass filtering occur in the muscles, having a large effect on SNR. The first stage has its effect on the membrane potential, and the second on the internal calcium concentration. Coupling results in a small further improvement due to a small change in the effective input impedance.

4. Conclusions and discussion

We have presented a first detailed electrophysiological model of *C. elegans* body wall muscles. We use this model to test several hypotheses about the possible role of these muscle cells in the locomotion of the worm. Model parameters were found such that the membrane properties of the cell bodies match experimental recordings. A possible caveat on those parameters is the lack of relevant *in vivo* data to date. Nonetheless, the model presented is likely to provide a valid first approximation of muscle behaviour in a behaving worm.

First, we rule out the possibility of calcium action potentials for parameters anywhere within the ballpark of the model we have presented. The fact that conductances would have to increase many fold to yield any oscillations in the model cells suggests that such behaviour is unlikely *in vivo*. This is an interesting result and contrasts with reported results for the related nematode worm, *Ascaris suum*. That said, the absence of action potentials in body wall muscles does not, in itself, preclude a possible role of these muscle cells in rhythmic pattern generation. (Indeed, there are no known action potentials in the interneurons and motor neurons of the locomotion system either.)

To determine the possible roles of muscle cells, first, in pattern generation, and second, in the propagation of signals along the worm, we present simulations of chains of coupled muscle cells (modeling a single quadrant of body wall muscles in the worm) and pairs of coupled muscle cells (modeling interquadrant coupling). In these simulations, the limiting factor is the strength of the gap junctional coupling. In fact, it appears that the reported conductance values are too low to support effective signal transmission between adjacent muscle cells. Hence, all of the results presented strongly suggest that in fact, *C. elegans muscles* are most likely to act only as actuators, and are not capable of communicating signals in a sufficiently effective manner, either to participate in pattern generation, or to propagate electrical oscillations.

It has been suggested that these body wall muscle cells also possess so called stretch receptor channels, that depolarise the cell in response to bending or stretching of the body [28]. If so, in a rhythmically bending or undulating worm, the muscles may, in principle, have the capacity to respond to the alternating body posture actively (but still with graded potential changes) thus aiding and maintaining this oscillatory behaviour. Such a sensory-feedback mechanism mimics closely existing models of sensory feedback driving neuronal activation in the ventral cord [5,7,8]. However, if this were true, such a mechanism would operate effectively independently from any neuronally generated oscillations, since the only points of contact between muscles and the nervous system (the neuromuscular junctions) only allow information flow in one direction – from the neurons to the muscles. Thus, to be interesting (i.e. to contribute significantly to pattern generation), muscles distributed along the body of the worm would need to coordinate their oscillations. Here, we have demonstrated that the weakness of the gap junctional coupling precludes the communication of such signals along a chain of muscles.

As a direct consequence, the model and simula-

tions presented here strongly suggest that the neural circuit is the active component generating the rhythmic patterns of locomotion (though we shed no light on the neural mechanism of generating such patterns – whether via a central pattern generating circuit, or via sensory feedback from stretch receptor channels).

Another question is what role the muscles may have in shaping locomotion. Figure 5 shows that the waveform of activity in muscles closely follows the waveform of the input. This holds true both with and without inter-muscular coupling. The muscles therefore seem to effectively be actuators. The muscles exhibit extended dynamic range due to the concave I-V relationship shown in Figure 4 and are capable of some (very limited) low-pass filtering. This relatively simple interpretation of muscle function has important implications for any neural model. The muscles' transfer function suggests that it should be possible to infer neural activity patterns from muscle output. The extended dynamic range should, if anything, improve robustness to changes in levels of neural activity and stochastic neurotransmitter release. In fact, in the absence of muscle output traces from behaving locomoting worms, the development of an appropriate physical model of the worm [4,29] would make it possible to infer neural activity patterns from behavioural observations.

Finally we have shown that the phenotypes of unc-7 or unc-9 mutation, or of unc-9 RNAi, cannot be explained by our model in terms of muscle gap junctions. One may therefore speculate as to which gap junctions (elsewhere in the locomotion system) may account for the reduced velocity observed in these mutant and RNAi treated worms. A likely candidate is the gap junctional coupling between the forward locomotion command interneurons AVB and forward locomotion motor neurons of classes VB and DB. Interestingly, models of the neural control of forward locomotion [7,8] have also suggested that modulation of command input into these motor neurons can modulate locomotion velocity [8].

Appendix A. Model parameters

A.1. *Parameters for the muscle body*

Due to the complexity of the fitness landscape for these parameters, multiple iterations of the evolutionary algorithm produced similar, but non-identical parameter sets. One such set (the one used for the simulations in this paper) is presented in Table A.1.

Param.	Val.	Reported Val.	Param.	Val.	Reported Val.
C_A	$72.3pF$	$\pm 75pF$ [22]	C_B	$30pF$	$29.6pF$ [12]
g_{Ks}	$436SF^{-1}$	$399SF^{-1}$ [21]	V_{Ks}	$-64.3mV$	$-67.9mV$ [21]
g_{Kf}	$400SF^{-1}$	$423SF^{-1}$ [21]	V_{Kf}	$-55.0mV$	$-47.0mV$[21]
g_{Ca}	$220SF^{-1}$	$199SF^{-1}$ [22]	V_{Ca}	$49.1mV$	$50.0mV$ [22]
g_L	$19.3SF^{-1}$	$22SF^{-1}$ [12]	V_L	$10.0mV$	n/a
αCa	0.283	n/a	ϕCa	2.39×10^{-6}	n/a
$V_{0.5_n}$	$19.9mV$	n/a	k_n	$15.9mV$	n/a
$V_{0.5_p}$	$-8.1mV$	n/a	k_p	$7.4mV$	n/a
$V_{0.5_q}$	$-15.6mV$	n/a	k_q	$-10.0mV$	n/a
$V_{0.5_e}$	$-3.4mV$	n/a	k_e	$6.7mV$	n/a
$V_{0.5_f}$	$25.2mV$	n/a	k_f	$5.0mV$	n/a
$Ca_{0.5_h}$	$64.1e-9$	n/a	k_h	$-10\mu M$	n/a
τ_n	$25.0ms$	n/a	τ_p	$2.3ms$	n/a
τ_q	$150ms$	n/a	τ_e	$0.10ms$	n/a
τ_f	$151ms$	n/a	τ_{Ca}	$11.6ms$	n/a

Table A.1
Parameters for the muscle body obtained by fits to experimental traces (see text for detail). Reported values are given where possible. The two values of C_A and C_B were used in our simulations for compatibility with voltage- and current-clamp data [21,22] and coupling parameters [12] respectively.

A.2. *Muscle arm parameters*

We began by estimating values for the specific capacitance (C_m) and resistance (R_m) of the membrane, and the specific resistance of the cytoplasm (R_l). Using the standard value of $C_m = 1\mu F/cm^2$, a cell with $C = 30pF$ (as in [12]) should have a surface area of $3 \times 10^{-3}\, mm^2$. The same cell was reported to have $G_{in} = 1/R_{in} = 666ps$, so $R_m = 45 \times 10^3\, \Omega\, cm^2$. Finally a standard value of $R_l = 100\, \Omega\, cm$ was chosen. Approximating each muscle arm as a cylinder with $l = 10\mu m$ and $r = 0.75\mu m$ (which we divide into ten compartments), we obtain:

$$c_m = C_m 2\pi r l$$
$$r_m = \frac{R_m}{2\pi r l}$$
$$r_l = \frac{R_l l}{\pi r^2}\,.$$

The resulting parameter values are given in Table A.2.

N	c_m	r_m	r_l
10	$47\,fF$	$950\,G\Omega$	$570\,k\Omega$

Table A.2
Muscle arm compartment parameters, obtained from estimates of the cell properties and dimensions (see text).

A.3. *Coupling parameters*

As a conservative choice of g_{intra}, we used the peak value reported in Ref. [12]. The value of g_{inter} is the reported value of $75pS$ divided evenly across the five arms of each muscle cell. The remaining parameters set the voltage dependence of the intra-quadrant coupling and were obtained by curve fitting to the experimental G/V curve in [12]. The parameters are given in Table A.2.

g_{intra}	g_{inter}	$G_{\min}$	A	V_0
$370pS$	$15pS$	0.13	40	$60mV$

Table A.3
Intra- and inter-quadrant coupling parameters. g_{intra} and g_{inter} were reported [12]. The remaining parameters were obtained by curve fitting to Figure 2. B of Ref. [12].

Appendix B. Calculating signal-to-noise ratio

We use spectral methods to calculate the signal-to-noise ratio (SNR) in a model muscle cell, stimulated with a superposition of a sinusoidal wave and white Gaussian noise. The input signal we use has a period $T = \dfrac{2\pi}{\omega_{\text{in}}} = 2s$. Simulations were run for a total duration of $D = 8s$ with a time step of $\Delta t = 0.01ms$.

The SNR is estimated from the power spectrum density (PSD) of the muscle output. For a signal $x(t)$, the PSD is given by

$$\text{PSD}(\omega) = X(\omega)X^*(\omega)/N\,,$$

where $X(\omega)$ is the Fourier transform of the signal (calculated with a fast Fourier transform or FFT, with $N = 2^{19}$, and the asterisk denotes complex conjugation.

To estimate the SNR from the PSD, we must first specify what frequency range will be considered "signal". Ideally the input should appear in the frequency domain as a spike of zero width at $0.5\,Hz$. In reality the signals (particularly the "filtered" signals V_i and $[Ca^{2+}]i$) will be smeared to some extent, leading to a peak of nonzero width. Based on visual inspection of the PSD, we have assigned all components on the range $0-5\,Hz$ to the signal, and from $5\,Hz$ to $50\,kHz$ to noise. While there will be some noise in the $0-5Hz$ range, this represents only 0.1% of the total bandwidth, and will not significantly affect the results. Finally we obtain values for the signal power, P_{signal}, the noise power P_{noise} and the ratio SNR as follows

$$P_{\text{signal}} = \frac{1}{N}\Sigma_{-5Hz}^{5Hz}\text{PSD}(\omega)$$
$$P_{\text{noise}} = \frac{1}{N}\left[\Sigma_{5Hz}^{50kHz}\text{PSD}(\omega) + \Sigma_{-50kHz}^{-5kHz}\text{PSD}(\omega)\right]$$
$$\text{SNR} = \frac{P_{\text{signal}}}{P_{\text{noise}}}\,.$$

The SNR is then calculated for different values of the input noise variance.

References

[1] D. L. Riddle, T. Blumenthal, B. J. Meyer, J. R. Priess (Eds.), *C. elegans* II, 2nd Edition, Cold Spring Harbour Laboratory Press, New York, 1997.

[2] C. elegans Sequencing Consortium, Genome sequence of the nematode *C. elegans*: A platform for investigating biology, Science 282 (1998) 2012–2018.

[3] J. G. White, E. Southgate, J. N. Thomson, S. Brenner, The structure of the nervous system of the nematode *Caenorhabditis elegans*, Philosophical Transactions of the Royal Society of London, Series B 314 (1986) 1–340.

[4] P. Erdös, E. Niebur, The neural basis of the locomotion of nematodes, Lecture Notes in Physics 368 (1990) 253–267.

[5] E. Niebur, P. Erdös, Theory of the locomotion of nematodes: Control of the somatic motor neurons by interneurons, Mathematical Biosciences 118 (1993) 51–82.

[6] J. A. Bryden, A simulation model of the locomotion controllers for the nematode *Caenorhabditis elegans*, Master's thesis, University of Leeds (2003).

[7] J. A. Bryden, N. Cohen, A simulation model of the locomotion controllers for the nematode *Caenorhabditis elegans*., in: S. Schaal, A. J. Ijspeert, A. Billard, S. Vijayakumar, J. Hallam, J. A. Meyer (Eds.), Proceedings of the eighth international conference on the simulation of adaptive behaviour, MIT Press / Bradford Books, 2004, pp. 183–192.

[8] J. A. Bryden, N. Cohen, Neural control of *C. elegans* forward locomotion: The role of sensory feedback, submitted.

[9] M. Suzuki, T. Tsuji, H. Ohtake, A model of motor control of the nematode *C. elegans* with neuronal circuits, Artificial Intelligence in Medicine 35 (2005) 75–86.

[10] D. A. Weisblat, R. L. Russell, Propagation of electrical activity in the nerve cord and muscle syncytium of the

nematode *Ascaris lumbricoides*, Journal of comparative Physiology 107 (1976) 293–307.
[11] P. Phelan, T. A. Starich, Innexins get into the gap, BioEssays 23 (2001) 388–396.
[12] Q. Liu, B. Chen, E. Gaier, J. Joshi, Z. W. Wang, Low conductance gap junctions mediate specific electrical coupling in body-wall muscle cells of *Caenorhabditis elegans*, Journal of Biological Chemistry 281 (2006) 7881–7889.
[13] G. B. Ermentrout, n:m phase-locking of weakly coupled oscillators, Journal of Mathematical Biology 12 (1981) 327–342.
[14] B. D. Ermentrout, N. Kopell, Frequency plateaus in a chain of weakly coupled oscillators, I., SIAM Journal of Mathematical Analysis 15 (1984) 215–237.
[15] N. Kopell, G. B. Ermentrout, Symmetry and phaselocking in chains of weakly coupled oscillator, Communications on Pure and Applied Mathematics 39 (1986) 623–660.
[16] A. Sherman, J. Rinzel, Rhythmogenic effects of weak electrotonic coupling in neuronal models, Neurobiology 89 (1992) 2471–2474.
[17] A. K. Han, C. Kurrer, Y. Kuramoto, Dephasing and bursting in coupled neural oscillators, Physical Review Letters 75 (1995) 3190–3193.
[18] D. Ramana Reddy, A. Sen, G. L. Johnston, Time delay induced death in coupled limit cycle oscillators, Physical Review Letters 80 (1998) 5109–5112.
[19] N. Cohen, The development of spontaneous beating activity in cultured heart cells: from cells to networks, Ph.D. thesis, Israel Institute of Technology, Kislev, 5761, Haifa (December 2000).
[20] S. J. Dixon, P. J. Roy, Muscle arm development in *Caenorhabditis elegans*, Development 132 (2005) 3079–3092.
[21] M. Jospin, M. C. Mariol, L. Segalat, B. Allard, Characterisation of K+ currents using an *in situ* patch clamp technique in body wall muscle cells from *Caenorhabditis elegans*, Journal of Physiology 544.2 (2002) 373–384.
[22] M. Jospin, V. Jacquemond, M. C. Mariol, L. Segalat, B. Allard, The l-type voltage-dependent Ca2+ channel EGL-19 controls body wall muscle function in *Caenorhabditis elegans*, Journal of Cell Biology 159 (2002) 337–347.
[23] K. Price, R. Storn, Differential evolution, Dr. Dobb's Journal April (1997) 18–24.
[24] R. E. Davis, A. O. W. Stretton, Signalling properties of *Ascaris* motorneurons: Graded active responses, graded synaptic transmission, and tonic transmitter release, Journal of Neuroscience 9 (1989) 415–425.
[25] D. A. Weisblat, L. Byerly, R. L. Russel, Ionic mechanisms of electrical activity in somatic muscle of the nematode *Ascaris lumbricoides*, Journal of comparative Physiology 111 (1976) 93–113.
[26] B. Allard, Personal Communication (2006).
[27] J. E. Richmond, E. M. Jorgensen, One GABA and two acetylcholine receptors function at the *C. elegans* neuromuscular junction, Nature neuroscience 2 (1999) 791–797.
[28] J. Liu, B. Schrank, R. H. Waterston, Interaction between a putative mechanosensory membrane channel and a collagen, Science 273 (1996) 361–364.
[29] J. H. Boyle, J. Bryden, N. Cohen, An integrated neuromechanical model of *C. elegans* forward locomotion, submitted.